



Stress Evolution on the Phase Boundary in LiFePO₄ Particles

Cheng-Kai ChiuHuang and Hsiao-Ying Shadow Huang^z

Mechanical and Aerospace Engineering Department, North Carolina State University, Raleigh,
North Carolina 27695, USA

It is commonly thought that diffusion-induced stress is one of the main factors causing loss of capacity in electrode materials. To understand stress evolution on the phase boundary during the lithiation process, we develop a finite element model adopting lithium ion concentration-dependent anisotropic material properties and volume misfits. Increased mechanical stresses on the phase boundaries are observed during the lithiation process. When the particle is more fully lithiated, larger stresses occur on the free surfaces and these may be related to the cracks on the *ac*-plane. The C-rate dependent strain energy evolution is also studied. The result shows that with the same amount of lithiation, particles experience different strain energies due to varied C-rate discharging. The high elastic energy from the high C-rate model suggests that the system becomes unstable, and a homogeneous phase transformation path is more plausible for the system. The current study provides a connection between diffusion-induced stresses on the phase boundary and the cracking propensity on free surfaces. Thus, the study could be used to better understand the mechanisms that cause particle fracture and capacity loss.

© 2013 The Electrochemical Society. [DOI: 10.1149/2.079311jes] All rights reserved.

Manuscript submitted June 20, 2013; revised manuscript received September 26, 2013. Published October 8, 2013.

Due to their high energy density, lithium-ion batteries are currently preferred as the main energy storage devices for PHEVs/EVs.^{1,2} However, retaining the lithium-ion battery capacity is one of the major challenges facing the electrochemical community today. Capacity loss is found in several conditions, such as at a high (dis)charging rate² or with long periods of cycling,³ and the capacity fade is strongly related to the mechanical stresses inside the materials.^{4,5} Among many cathode materials, the olivine-based LiFePO₄ with an orthorhombic crystal structure provides excellent characteristics for application in EVs/PHEVs such as: good thermal stability, abundant iron resource, low raw material cost, and high theoretical energy density (170 mAh/g).⁵ However, electronic conductivity and diffusivity for LiFePO₄ are considerably lower than those of LiMn₂O₄ and LiCoO₂ materials,^{6,7} and these intrinsic disadvantages of LiFePO₄ are currently improved by doping, carbon coating, nano-scale particle size, or synthesis controls.^{5,8-10} Nevertheless, an understanding of the fundamental mechanisms resulting in capacity loss needs to be obtained, and it will hopefully culminate in breakthroughs in lithium-ion battery technology via synergistic investigative activities that bridge theory, computation, experiment, and manufacturing.

It has been reported that the electrochemically cycled LiFePO₄ under low C-rate exhibits a two-phase system:¹¹⁻¹⁴ lithium-rich (LiFePO₄) and lithium-poor (FePO₄) phases. These two phases have similar crystal structures and are constrained by a coherent interface during the phase transformation.¹⁵ Because of different lattice constants for the two phases, approximately 7–9% volume misfits are observed.¹⁶ Moreover, computational simulations and experimental observations have identified that lithium ion diffusion in LiFePO₄ is one-dimensional and confined along the *b*-axis.¹⁷⁻²¹ Chen et al.²² have studied the phase boundary via high resolution transmission electron microscopy, and two phases separated by a visible disordered zone on the *bc*-plane were observed. On the other hand, Laffont et al.²³ have reported a nano-sized interfacial zone (ca. 8–22 nm), and it is always found in a partially lithiated/delithiated particle with sizes of 130, 170 or 172 nm. It is concluded that the phase boundary tends to move along the *a*-axis with the extension of the pre-existing phase. Later, Delmas et al.²⁴ proposed a domino-cascade model to explain the intercalation/extraction of lithium ions in a single particle based on the assumption that a mixture of particles in a discharging sample are either fully lithiated or delithiated. It is suggested that the phase boundary propagation wave along the *a*-axis is formed because of the relatively low energy barrier in the distorted interfacial area. The model was later confirmed experimentally by Brunetti et al.,²⁵ showing that most particles ranging from 50 nm to 300 nm in a partially charged lithium-ion cell sample are either in a fully LiFePO₄ phase or a FePO₄ phase.

Meethong et al.¹² and Tang et al.^{26,27} discussed the role of the coherency-induced elastic energy during the phase transformation by incorporating spherical particles. Van der Ven et al.²⁸ studied the role of coherent strains on the phase stability of needle crystallites and it was concluded that the minimum strain energy could be maintained by decreasing the interfacial area on the *bc*-plane between two phases. By incorporating anisotropic volume expansions during the phase transformation, Tang et al.²⁹ and Cogswell et al.^{30,31} utilized a phase field method to study changes in the phase boundary morphology on plate-like particles. However, concentration-dependency of material properties and volume misfits were not included. In contrast, Deshpande et al.³² adopted an isotropic core-shell model while incorporating concentration-dependent elastic moduli to study diffusion-induced stresses, and it is suggested that material stiffening is beneficial for avoiding surface cracking. However, their model considered isotropic diffusion and phase boundary movements.³² Moreover, other intercalated electrode materials, such as LiCoO₂ and LiMn₂O₄, have also been extensively studied,^{33,34} specifically the studies focused on developing mathematical models to delineate diffusion-induced stresses and interphase stresses due to phase boundary movement.

Despite the collective studies, it is absolutely necessary and timely to study the diffusion-induced stresses in LiFePO₄ as a whole: the anisotropic directions of the diffusion and the phase movement should be incorporated, and the concentration-dependency of anisotropic material properties and volume expansions should be considered. Therefore, in the current study we use a single plate-like LiFePO₄ particle with the aforementioned anisotropic properties as our model system to investigate the mechanical stress evolution, specifically on the phase boundary during the lithiation process. We relate our stress fields at the different lithiation stages to the fracture tendency in the particle, and we compare the strain energy variation at different C-rates. The results from the current study could be used to provide a better understanding of mechanisms that interface lithium ion diffusion, stresses on the phase boundary, fracture propensity, and C-rates.

Method

We use a thermal stress analysis approach to investigate diffusion-induced stress evolution at the two-phase boundary during the lithiation process, whereas the thermal diffusivity mimics the lithium-ion diffusivity, and the temperature gradient represents the lithium-ion concentration gradient. The anisotropic diffusion-controlled model is considered in the current study.^{29,35} ANSYS finite element software (ANSYS, Inc., Canonsburg, Pennsylvania, USA) is incorporated and a plate-like LiFePO₄ single particle with dimensions of 150 nm × 60 nm × 100 nm is developed (Figure 1); the particle size is designed to be within the range of experimental observation.²³⁻²⁵ The finite element model containing 3780 elements is divided into 10 layers along the

^zE-mail: hshuang@ncsu.edu

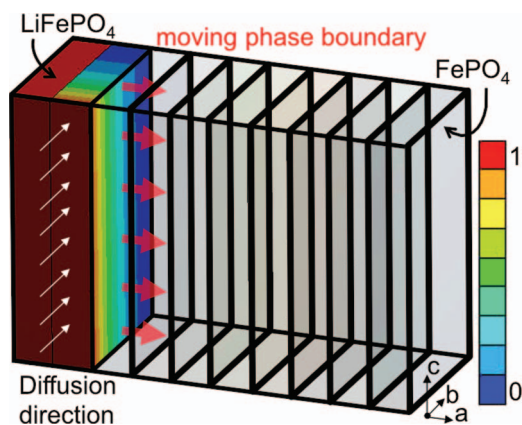


Figure 1. A plate-like Li_xFePO_4 single particle finite element model with a dimension of $150 \text{ nm} \times 60 \text{ nm} \times 100 \text{ nm}$, where lithium ions diffuse along the b -axis and the phase boundary moves along the a -axis. The model is divided into 10 layers along the a -axis, and each layer represents one lithium ion diffusion channel. Colored legend: High lithium ion concentration is in red and low lithium ion concentration is in blue.

a -axis and each layer represents one lithium-ion diffusion channel, whereas each channel contains 378 elements along the b -axis. A 10-step finite element analysis is designed, such that each step represents diffusion in each channel.

The anisotropic diffusion-controlled analysis requires a set of boundary and initial conditions for each channel: a unit of concentration on one surface $\phi(y, t) = \phi(0, t) = 1$, and a zero-concentration on the other surface at the end of the said channel $\phi(y, t) = \phi(1, 0) = 0$ (Figure 1), where ϕ is the concentration, y is the diffusion length along the b -axis, and t is the time required for the completion of the diffusion. The time-dependent concentration gradient serves as the driving force of the diffusion for the phase transformation,^{33,36,37} and it is described by the governing equation: $\frac{\partial \phi}{\partial t} = D \left(\frac{\partial^2 \phi}{\partial y^2} \right)$. That is, the Fick's second law of diffusion, where D is the diffusivity. The concentration-independent diffusivity along the b -axis is defined as $D_b = 1\text{E-}15 \text{ m}^2/\text{s}$ obtained from Park et al.⁷ Since studies have shown that lithium-ion hopping between channels is very unlikely,³⁸ and to ensure the anisotropic diffusivity, the diffusivities of the other two directions are set to be 10-order of magnitude smaller comparing to the one along the b -axis: $D_a = D_c = 1\text{E-}25 \text{ m}^2/\text{s}$. It is to ensure that lithium ions move smoothly and systematically from high-concentration regions (in red) to low-concentration regions (in blue) within channels (Figure 1).

For each step of the finite element analysis, the completion of the diffusion for each channel is reached when the concentration $\phi(y, t) = \phi(1, 1) = 1$ at the end of the channel. It is immediately followed by the next analysis in the adjacent channel, where boundary and initial conditions (i.e., $\phi(y, t) = \phi(0, t) = 1$ and $\phi(y, t) = \phi(1, 0) = 0$) are assigned in the said channel and the Fick's second law of the diffusion is again applied. A total of 10 steps of finite element analysis complete the lithiation of Li_xFePO_4 , where x represents lithiated percentages ($0\% \leq x \leq 100\%$).

Concentration-dependent anisotropic material properties and volume expansions for Li_xFePO_4 are incorporated: anisotropic material property matrices $[C]$ and the volume expansion (α) are defined as follows: $[C(x)] = x[C]^{\text{LiFePO}_4} + (1-x)[C]^{\text{FePO}_4}$ and $\alpha_i(x) = x\alpha_i^{\text{LiFePO}_4}$, where $i = a, b$, and c representing lattice vectors. Orthorhombic elastic constants for both the lithium-rich and lithium-poor phases are obtained from the reference.³⁹ The anisotropic volume expansions of the LiFePO_4 phases are obtained from the literature,^{12,16} in which $\alpha_a = 5.8\%$, $\alpha_b = 4.5\%$, and $\alpha_c = -1.3\%$. These two material properties are incorporated into the 10-step finite element analysis. For example, at the 60% of the lithiation of one specific channel, the anisotropic material property matrix is a linear com-

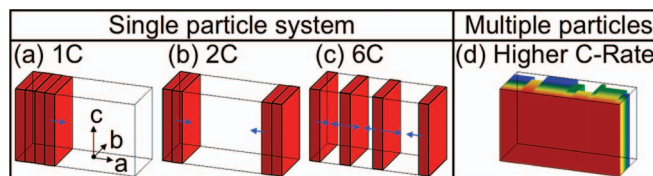


Figure 2. Particles with 40% lithiation at different C-rates. (a) A sequential phase transformation path for the 1C model is considered.²⁴ (b)-(c): High C-rate phase transformation models utilize the approach proposed by Singh et al.,³⁵ where the number of phase boundaries is proportional to the C-rate. (d) A representative multiple particle system at a high C-rate: lithium ions diffuse in multiple channels or in the ac -plane simultaneously. Colored legend: High lithium ion concentration is in red and low lithium ion concentration is in blue.

position of two phases: $[C(60\%)] = 0.6[C]^{\text{LiFePO}_4} + 0.4[C]^{\text{FePO}_4}$. The LiFePO_4 phase is subjected to anisotropic volume expansions as follows: $\alpha_a = 60\% \alpha_a^{\text{LiFePO}_4} = 60\% \times 5.8\% = 3.48\%$, $\alpha_b = 60\% \alpha_b^{\text{LiFePO}_4} = 60\% \times 4.5\% = 2.7\%$, and $\alpha_c = 60\% \alpha_c^{\text{LiFePO}_4} = 60\% \times (-1.3\%) = -0.78\%$.

C-rate dependent lithiation and the associated phase transformation paths are studied. Coherent interfaces are imposed between phases and are assumed to be defect free in our finite element models. In our finite element analyzes, a sequential phase transformation path for the lower C-rate is considered (Figure 2a). The LiFePO_4 phase initially nucleates in channel 1 as such locations exhibit less interfacial area between two phases (e.g. at corners)²⁹ and the phase nucleation is along the shortest diffusion length (along the b -axis for LiFePO_4).^{18,23,40} Thus, a domino-cascade model is used for 1C finite element models, as there is no energy barrier in the interfacial region between two phases.²⁴

For high C-rates, we follow models proposed by Singh et al.,³⁵ where the number of phase boundaries is proportional to the number of the C-rate (Figure 2b-2c). That is, the second phase is formed at two different locations to provide two phase-boundary for the 2C model, and the second phase is formed at four different locations to provide six phase-boundary for the 6C model. Such assumption is based on the surface-reaction-limited dynamics describing that the phase boundary advances by filling channels sequentially in the crystal. It is claimed that while more phase boundaries are formed, it allows more lithium being inserted/extracted from the particle and thus provides higher currents.³⁵

The stress field on the phase boundary at different percentages of lithiation is studied, and strain energies during lithiation with different C-rates are also compared. A proposed multiple particle system with a higher C-rate is discussed in the next section (Figure 2d). In the current study, the strain energy reported from the finite element analysis is formulated as $U = \int \sigma d\epsilon$, where σ is the diffusion-induced stress field, and ϵ is the corresponding strain field. The strain field is related to the deformation of the model due to concentration-dependent anisotropic volume expansions. The total strain energy U is the summation of the strain energy of each element. The post-processing of ANSYS is with a built-in capability to output the total strain energy based on the individual strain energy of each element. The stress analysis consists 10 steps for a complete lithiation, and for each step, there are several time increments to ensure the completion of the diffusion in each channel. In the current study, we obtain the stress field and the total strain energy at each time increment and for each analysis step, until the particle is fully lithiated.

Results and Discussion

Normalized stress fields on the phase boundary (yz -plane or bc -plane) at different percentages of lithiation for the 1C model are compared: initial, 10%, 20%, 50%, 60%, 80%, and 90% lithiation (Figures 3 and 4). Specifically, Figure 3a, 3g, and 3m represent stress fields on the phase boundary between channels one and two upon lithiation. When reaching 10% lithiation, the resultant stress fields on the phase boundary between channels 1 and 2 are shown in

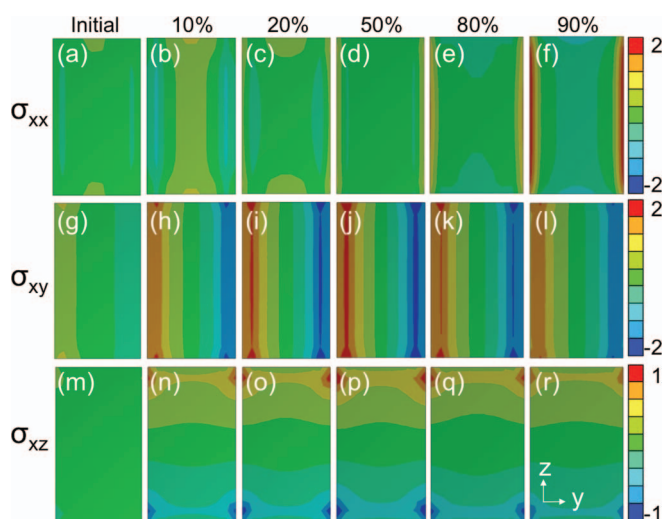


Figure 3. A representative normalized stress field on phase boundaries at different lithiation stages for the 1C model. (a)-(f): the particle is in compression (σ_{xx}) at low lithiation stages and in tension at high lithiation stages. This is due to the volume misfit of the two phases and the coherent interface. (g)-(l) High in-plane shear stresses (σ_{xy}) along the particle surfaces are observed, and the results suggest that particles are subjected to the highest σ_{xy} at 50% lithiation. (m)-(r): Lithiation-independent in-plane shear stresses σ_{xz} are uniformly distributed on the phase boundary and corners are subjected to higher mechanical stresses. Colored legend: Tension is in red and compression is in blue.

Figure 3b, 3h and 3n. Moreover, after completing 50% lithiation, the resultant stress fields on the phase boundary between channels 5 and 6 are shown in Figure 3d, 3j, and 3p. Increased mechanical stresses at the phase boundaries are observed during the lithiation process.

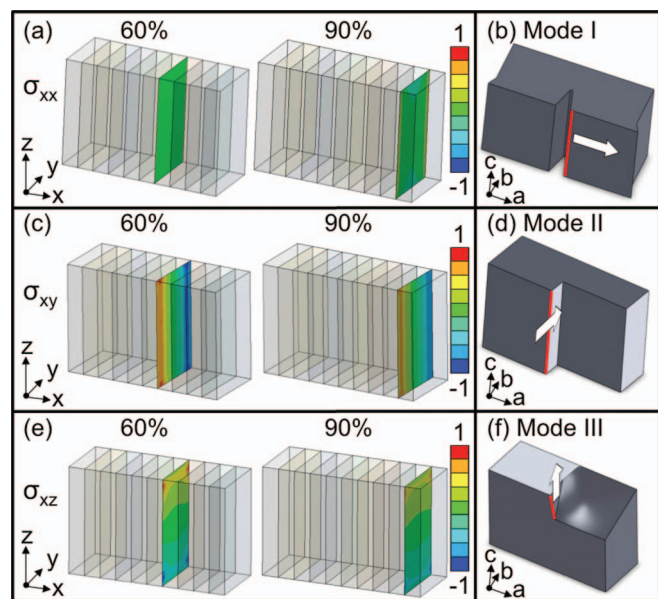


Figure 4. A representative normalized stress field on the phase boundary at different lithiation stages for the 1C model. An initial crack at the surface of the particle under repetitive (dis)charging cycles could lead to Modes I, II, and III fractures. (a)-(b) When the particle is more than 60% lithiated, larger σ_{xx} tension exists on the free surface parallel to the z -axis, suggesting that a Mode I fracture might occur if an initial flaw (presented in color red) exists on the ac -plane. (c)-(d) Large σ_{xy} exists on the yz -plane parallel to the phase boundary, suggesting that a Mode II fracture could occur. (e)-(f) Lithiation-independent σ_{xz} on the phase boundary could lead to a Mode III fracture. Colored legend: Tension is in red and compression is in blue.

Concentration-dependent normal stresses σ_{xx} are observed, and these are due to molar volume misfits since two phases are constrained at a coherent interface¹² (Figure 3a-3f). It is observed that the particle is in compression (σ_{xx}) at the low lithiation stage (Figure 3a-3c) and is in tension beyond 50% lithiation in the current study (Figure 3d-3f and Figure 4a). Various studies have implemented core-shell models to investigate diffusion-induced stresses;^{32,33,41-44} of note, such geometry of the two phases (shell and core) within the particle prohibits sliding; therefore coherent interfaces do not exist between two phases. Among these collective work, Christensen et al.^{33,41} and Deshpande et al.^{32,42} have established analytical models describing stress profiles of the particle for different electrode materials during (de)lithiation. When solving the elasticity problem of the core-shell model, the diffusion-induced stress in the equilibrium equation is treated as the pressure (or a Lagrange multiplier) applying on the outer surface of the model.^{32,33,41,42} Such treatment is analogous to the Eshelby's inclusion problem⁴⁵ and the analytical solutions of the boundary value problem generally result in compression on the particle surface, specifically along the tangential direction. In contrast to these studies, the current work considers the coherent interface between two phases during lithiation, and this is the case for LiFePO_4 particularly.^{12,27,29-31,46,47} As such, additional residual stresses due to the coherent interface raises the system's potential energy and provides distinct stress profiles from studies based on core-shell models.^{32,33,41,42} Our study also shows that when the particle is toward fully lithiated (90%), larger tension occurs on the free surface parallel to the z -axis (Figures 3f and 4a), suggesting a crack opening might occur if an initial flaw exists on the ac -plane. Hence, lithium ion diffusion along the b -axis above 50% lithiation results in large normal stresses σ_{xx} and consequently a Mode I fracture is likely to occur if an initial flaw exists (Figure 4b).

The lithiation causes non-negligible shear stress σ_{xy} , specifically along the particle free-surfaces (Figures 3g-3l and 4c), suggesting that such high shears could be responsible for the observed surface cracking (Figure 4c-4d).^{22,48} It is observed that σ_{xy} increases when lithiating to 50% (Figure 3g-3j), and the shearing stress starts decreasing beyond 50% lithiation (Figures 3j-3l and 4c). This indicates that LiFePO_4 particles are subjected to the highest diffusion-induced shear stresses at the 50% lithiation stage. Furthermore, lithiation-independent σ_{xz} are uniformly distributed on the phase boundary (Figures 3m-3r and 4e). The shear stresses are observed with larger values at corners close to the free surfaces, indicating these locations are susceptible to fracture (Figure 4e-4f). The normalized stress field in Figures 3 and 4 is to delineate how each stress component is evolved during the lithiation process. Comparing stress magnitudes at 50% lithiation, $\sigma_{xx} : \sigma_{xy} : \sigma_{xz} = 0.67 \text{ GPa} : 1.8 \text{ GPa} : 0.7 \text{ GPa} = 1:3:1$, the result indicates that Mode II fracture is more likely to occur before other two modes. Taking together, the result in the current study provides a connection between diffusion-induced stresses at the phase boundary and the cracking propensity on the ac -plane. Should an initial crack form at the surface of the particle as observed,^{22,48} fracture mechanics ought to be used to study associated stress intensity factors and energy release rates.⁴⁹ To investigate the effects of internal stresses to a cracked particle, a finite element method-based virtual crack closure technique was conducted and the result is published elsewhere.⁵⁰ It is complementary to the study discussing three different lithium intercalation-induced dislocation mechanisms for experimentally observed cracks.⁵¹ Moreover, Woodford et al. have developed a fracture mechanics failure criterion of a single particle and polycrystals;^{52,53} The "electrochemical shock" has provided design criteria for several electrode material systems (Li_xCoO_2 , $\text{Li}_{1+x}\text{Mn}_2\text{O}_4$, $\text{Li}_x\text{Ni}_{0.8}\text{Co}_{0.15}\text{Al}_{0.05}\text{O}_2$, $\text{Li}_x\text{Ni}_{1/3}\text{Co}_{1/3}\text{Mn}_{1/3}\text{O}_2$) in which minimizing the diffusion-induced principal shear strain is of paramount importance for long-lived battery electrodes.^{52,53}

The C-rate dependent strain energy evolution during lithiation is shown in Figure 5. The 1C model is inspired by Delmas et al.²⁴ and high C-rate finite element models utilize the approach proposed by Singh et al.³⁵ The strain energy of the particle with 40% lithiation at different C-rates is also compared, as indicated by square markers (Figure 5). The result shows that with the same amount of

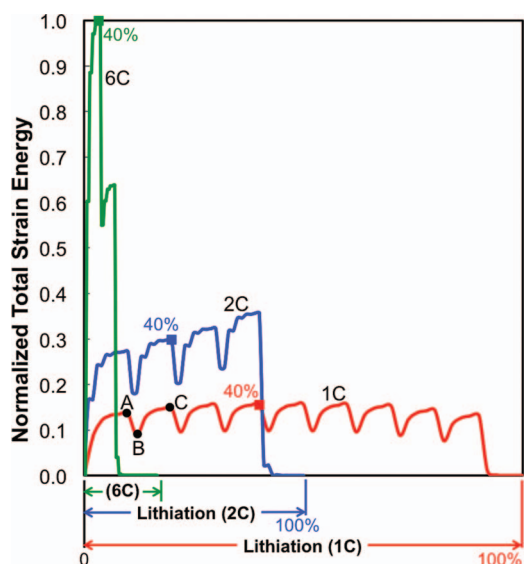


Figure 5. The C-rate dependent strain energy evolution during a complete lithiation cycle. The strain energies in the particles with 40% lithiation are indicated by square markers. The 1C model uses a sequential phase transformation path proposed by Delmas et al.²⁴ and high C-rate models are inspired by Singh et al.³⁵ The high elastic energy from the 6C model suggests that the existence of multiple coherent interfaces within a particle could be unstable,^{54,59} and therefore Singh's approach is not plausible thermodynamically. As a result, lithium ion diffusion in multiple channels or in the *ac*-plane simultaneously are more plausible for the high C-rate model, as shown in Figure 4d.

lithiation (Figure 2a-2c), particles experience different strain energies at different C-rate discharging. For the 1C model, there being nine complete phase boundaries formed during different stages of lithiation (Figures 1 and 5). Similarly, four and two repetitive fluctuations during the strain energy evolution are observed in the 2C and 6C models, respectively (Figure 5). The results indicate that the strain energy increases when lithium ions diffuse into the channel, i.e., during the two-phase region. The completion of the diffusion at each channel forms a complete phase boundary between two single phases. That is, the coherency results in local maximum volume misfits, which in turns generating high strain energy inside the particle, shown as the point A in Figure 5. Upon lithiation in the adjacent channel, LiFePO₄ phase starts nucleating accompanying with most of FePO₄ phase in the rest of the channel and the particle. As such, the reduction of the complete phase boundary results in the relaxation of the strain energy, shown as the point B in Figure 5. Strain energy increases again due to the coherency between two phases and reaches its local maximum once the diffusion is completed in the said channel (the point C in Figure 5). Of note, the total strain energy at the point C is comparable to the one at the point A and it is mainly attributed to the total number of phase boundary remaining in the particle. Similar trend is also observed for higher C-rate simulation.

From a thermodynamic point of view, the energy fluctuations during the lithiation process suggest that the Gibbs comment tangent rule is not applicable when a coherent interface is present, as previously discussed by Cahn, Voorhees, Johnson, and Bazant.^{30,31,54-56} Briefly, in the current study, a two-component isothermal system, whereas phase behaviors in coherent equilibria is considered. A molar free energy is used to present the chemical equilibrium initially without the coherency, and a solid-solid coherency between two phases is included and thus raises the potential energy of the system. Due to the existence of the coherency, the mole fractions of the phases are no longer smooth functions of the average composition of the alloy.^{54,57} The existence of the strain energy raises the potential energy of the system and therefore, the comment tangent rule becomes invalid in the two-phase region. Furthermore, a few experimental studies have confirmed that particles are either in FePO₄ or LiFePO₄ phases under low

C-rate (dis)charging,^{24,25,58} as solid solutions provide lower energy barriers for thermodynamic equilibrium. Therefore, the high elastic energy from the 6C model suggests that the existence of multiple coherent interfaces within a particle could be unstable,^{54,59} as the raised potential energy is too large and lies above the free energy curve. As a result, the models from Singh et al.³⁵ propose that the number of phase boundaries is proportional to the C-rate (Figure 2b-2c) are not plausible thermodynamically. Moreover, several studies have shown that for fast (dis)charging, LiFePO₄ material does not demonstrate a two-phase system.² Therefore, the calculated high strain energy for the 6C model suggests that another phase transformation path is preferred: a homogeneous phase transformation toward the suppression of a two-phase system in a LiFePO₄ particle is more energetically favorable (Figure 2d), as discussed by Bazant.^{30,31}

As such, we are currently studying the stress evolution in multiple particles under higher C-rate discharging, in which the concentration dependency of materials properties and volume expansions are also considered. Specifically, lithium ion diffusion in multiple channels or in the *ac*-plane simultaneously are considered, whereas an increased number of incomplete phase boundaries exist in the system (Figure 2d). The result from our current study indicates that coherency between two phases plays an important role in the variation of the mechanical strain energy within the particle. As for a larger system, (i.e., multiple particles under higher-C-rate), incomplete phase boundaries are generally reported.^{2,58,60} Therefore, it is expected that there are less coherency inside the particles and less mechanical strain energy fluctuation for a larger system.

Conclusion

A diffusion-controlled finite element model accompanied with the experimentally observed phase boundary propagation is developed, in which concentration-dependent anisotropic material properties and volume misfits are incorporated. Increased mechanical stresses on the phase boundaries are observed during the lithiation process. Specifically, normal stress σ_{xx} and shear stresses σ_{xy} and σ_{xz} on the phase boundary are at their highest values on the free surfaces of the phase boundary. These diffusion-induced stresses could possibly lead to the occurrence of Mode I, Mode II, and Mode III fractures if an initial crack exists on the *ac*-plane. Thus, the current study provides important complementary data about the cracking propensity in LiFePO₄ particles, and we believe it is strongly related to the observed capacity loss. In addition, C-rate dependent strain energy evolution and fluctuation are also studied. The result indicates that coherency between two phases plays an important role in the variation of the mechanical strain energy within the particle. It is also observed that with the same amount of lithiation, particles experience different strain energies due to varied C-rate discharging. The large elastic energy from the high C-rate model suggests that the existence of multiple coherent interfaces within a particle could be unstable since the total energy becomes too large and lies above the free energy curve. Therefore, lithium ions diffusion in multiple channels or in the *ac*-plane simultaneously are more plausible for higher C-rate models.

References

1. Y.-M. Chiang, *Science*, **330**, 1485 (2010).
2. B. Kang and G. Ceder, *Nature*, **458**, 190 (2009).
3. Y. C. Zhang, C. Y. Wang, and X. D. Tang, *Journal of Power Sources*, **196**, 1513 (2011).
4. J. B. Goodenough and Y. Kim, *Chemistry of Materials*, **22**, 587 (2010).
5. L.-X. Yuan, Z.-H. Wang, W.-X. Zhang, X.-L. Hu, J.-T. Chen, Y.-H. Huang, and J. B. Goodenough, *Energy & Environmental Science*, **4**, 269 (2011).
6. Y. Wang and H.-Y. S. Huang, *TSEST Transaction on Control and Mechanical Systems*, **1**, 192 (2012). <http://tsest.org/index.php/TCMS/article/view/61/36>.
7. M. Park, X. Zhang, M. Chung, G. B. Less, and A. M. Sastry, *Journal of Power Sources*, **195**, 7904 (2010).
8. S. Y. Chung, J. T. Bloking, and Y. M. Chiang, *Nature Materials*, **2**, 702 (2003).
9. S.-Y. Chung, J. T. Bloking, and Y.-M. Chiang, *Nature Materials*, **1**, 128 (2002).
10. W.-J. Zhang, *Journal of Power Sources*, **196**, 2962 (2011).

11. N. Meethong, Y.-H. Kao, M. Tang, H.-Y. Huang, W. C. Carter, and Y.-M. Chiang, *Chemistry of Materials*, **20**, 6189 (2008).
12. N. Meethong, H.-Y. S. Huang, S. A. Speakman, W. C. Carter, and Y.-M. Chiang, *Advanced Functional Materials*, **17**, 1115 (2007).
13. N. Meethong, H.-Y. S. Huang, W. C. Carter, and Y.-M. Chiang, *Electrochemical and Solid State Letters*, **10**, A134 (2007).
14. Y.-H. Kao, M. Tang, N. Meethong, J. Bai, W. C. Carter, and Y.-M. Chiang, *Chemistry of Materials*, **22**, 5845 (2010).
15. N. Meethong, Y.-H. Kao, S. A. Speakman, and Y.-M. Chiang, *Advanced Functional Materials*, **19**, 1060 (2009).
16. G. Rousse, J. Rodriguez-Carvajal, S. Patoux, and C. Masquelier, *Chemistry of Materials*, **15**, 4082 (2003).
17. S. E. Boulfelfel, G. Seifert, and S. Leoni, *Journal of Materials Chemistry*, **21**, 16365 (2011).
18. S.-i. Nishimura, G. Kobayashi, K. Ohoyama, R. Kanno, M. Yashima, and A. Yamada, *Nature Materials*, **7**, 707 (2008).
19. R. Malik, D. Burch, M. Bazant, and G. Ceder, *Nano Letters*, **10**, 4123 (2010).
20. G. K. P. Dathar, D. Sheppard, K. J. Stevenson, and G. Henkelman, *Chemistry of Materials*, **23**, 4032 (2011).
21. J. J. Yang and J. S. Tse, *Journal of Physical Chemistry A*, **115**, 13045 (2011).
22. G. Chen, X. Song, and T. J. Richardson, *Electrochemical and Solid-State Letters*, **9**, A295 (2006).
23. L. Laffont, C. Delacourt, P. Gibot, M. Y. Wu, P. Kooyman, C. Masquelier, and J. M. Tarascon, *Chemistry of Materials*, **18**, 5520 (2006).
24. C. Delmas, M. Maccario, L. Croguennec, F. Le Cras, and F. Weill, *Nat Mater*, **7**, 665 (2008).
25. G. Brunetti, D. Robert, P. Bayle-Guillemaud, J. L. Rouviere, E. F. Rauch, J. F. Martin, J. F. Colin, F. Bertin, and C. Cayron, *Chemistry of Materials*, **23**, 4515 (2011).
26. M. Tang, W. C. Carter, and Y.-M. Chiang, *Annual Review of Materials Research*, **40**, 501 (2010).
27. M. Tang, H. Y. Huang, N. Meethong, Y. H. Kao, W. C. Carter, and Y. M. Chiang, *Chemistry of Materials*, **21**, 1557 (2009).
28. A. Van der Ven, K. Garikipati, S. Kim, and M. Wagemaker, *Journal of the Electrochemical Society*, **156**, A949 (2009).
29. M. Tang, J. F. Belak, and M. R. Dorr, *Journal of Physical Chemistry C*, **115**, 4922 (2011).
30. P. Bai, D. A. Cogswell, and M. Z. Bazant, *Nano Letters*, **11**, 4890 (2011).
31. D. A. Cogswell and M. Z. Bazant, *Acs Nano*, **6**, 2215 (2012).
32. R. Deshpande, Y. Qi, and Y. T. Cheng, *Journal of the Electrochemical Society*, **157**, A967 (2010).
33. J. Christensen and J. Newman, *Journal of Solid State Electrochemistry*, **10**, 293 (2006).
34. S. Renganathan, G. Sikha, S. Santhanagopalan, and R. E. White, *Journal of the Electrochemical Society*, **157**, A155 (2010).
35. G. K. Singh, G. Ceder, and M. Z. Bazant, *Electrochimica Acta*, **53**, 7599 (2008).
36. X. Zhang, W. Shyy, and A. M. Sastry, *Journal of the Electrochemical Society*, **154**, A910 (2007).
37. Y. T. Cheng and M. W. Verbrugge, *Journal of Power Sources*, **190**, 453 (2009).
38. D. Morgan, A. Van der Ven, and G. Ceder, *Electrochemical and Solid State Letters*, **7**, A30 (2004).
39. T. Maxisch and G. Ceder, *Physical Review B*, **73**, 174112 (2006).
40. A. Yamada, H. Koizumi, S.-i. Nishimura, N. Sonoyama, R. Kanno, M. Yonemura, T. Nakamura, and Y. Kobayashi, *Nature Materials*, **5**, 360 (2006).
41. J. Christensen and J. Newman, *Journal of the Electrochemical Society*, **153**, A1019 (2006).
42. R. Deshpande, Y. T. Cheng, and M. W. Verbrugge, *Journal of Power Sources*, **195**, 5081 (2010).
43. R. Deshpande, M. Verbrugge, Y. T. Cheng, J. Wang, and P. Liu, *Journal of the Electrochemical Society*, **159**, A1730 (2012).
44. S. J. Harris, R. D. Deshpande, Y. Qi, I. Dutta, and Y. T. Cheng, *Journal of Materials Research*, **25**, 1433 (2010).
45. J. D. Eshelby, *Proceedings of the Royal Society of London Series a-Mathematical and Physical Sciences*, **241**, 376 (1957).
46. L. Li, X. Tang, H. Liu, Y. Qu, and Z. Lu, *Electrochimica Acta*, **56**, 995 (2010).
47. C.-K. ChiuHuang, M. A. Stamps, and H.-Y. S. Huang, *Materials Research Society Proceedings*, **1541**, F04 (2013).
48. H. Gabrisch, J. Wilcox, and M. M. Doeff, *Electrochemical and Solid State Letters*, **11**, A25 (2008).
49. Y. Hu, X. Zhao, and Z. Suo, *Journal of Materials Research*, **25**, 1007 (2010).
50. M. A. Stamps, J. W. Eischen, and H.-Y. S. Huang, *International Journal of Solids and Structures*, **Under Review** (2013).
51. H. Y. S. Huang and Y. X. Wang, *Journal of the Electrochemical Society*, **159**, A815 (2012).
52. W. H. Woodford, W. C. Carter, and Y. M. Chiang, *Energy & Environmental Science*, **5**, 8014 (2012).
53. W. H. Woodford, Y.-M. Chiang, and W. C. Carter, *Journal of the Electrochemical Society*, **157**, A1052 (2010).
54. J. W. Cahn and F. Larche, *Acta Metallurgica*, **32**, 1915 (1984).
55. P. W. Voorhees and W. C. Johnson, *Journal of Chemical Physics*, **90**, 2793 (1989).
56. W. Johnson and P. Voorhees, *Metallurgical and Materials Transactions A*, **18**, 1213 (1987).
57. F. C. Larche, F. Morgan, and J. Sullivan, *Scripta Metallurgica Et Materialia*, **24**, 491 (1990).
58. W. C. Chueh, F. El Gabaly, J. D. Sugar, N. C. Bartelt, A. H. McDaniel, K. R. Fenton, K. R. Zavadil, T. Tyliszczak, W. Lai, and K. F. McCarty, *Nano Letters*, **13**, 866 (2013).
59. R. O. Williams, *Calphad*, **8**, 1 (1984).
60. W. Dreyer, J. Jamnik, C. Gihlke, R. Huth, J. Moskon, and M. Gaberscek, *Nature Materials*, **9**, 448 (2010).